Indian Journal of Chemical Technology
Vol. 30, September 2023, pp. 634-642
DOI: 10.56042/ijct.v30i5.5206

Enhanced electrochemical performance of manganese oxide nanocomposites for supercapacitor application

K Kiruthika* & V Renuga

PG & Research Department of Chemistry, National College (autonomous),
Affiliated to Bharathidasan University, Tiruchirappalli-620001, Tamil Nadu, India

*E-mail: kiruthika.05@gmail.com

Received 1 March 2023; accepted 18 July 2023

Manganese oxide (MO) has been synthesised by chemical co-precipitation method and it was characterised for its functional group, phase structure, particle size and morphology by using FTIR, XRD, SEM and TEM. Additionally, its electrochemical properties like cyclic voltammetry (CV), galvanostatic charge/ discharge and electrochemical impedance spectroscopy (EIS) are recorded. The specific capacitance of the prepared manganese oxide is found to be 116 F/g at current density of 1 A/g. To augment its capacitance value, it was doped with multi-walled carbon nanotube (MWCNT) and poly(3,4-ethylenedioxythiophene) polystyrene sulfonate (PEDOT:PSS) and their electrochemical performance are recorded. By doping MWCNT and PEDOT:PSS over MO, a high specific capacitance of 537 F/g at a current density of 1 A/g with 97% capacitance retention and coulombic efficiency of 98% over 10,000 cycles at a current density of 5 A/g is obtained. All these results demonstrates that MO/MWCNT/PEDOT:PSS is a promising electrode material for supercapacitor application.

Keywords: Chemical co-precipitation, Manganese oxide, MWCNT, PEDOT:PSS, Supercapacitor, Energy storage

Due to the depletion of fossil fuels, change in climate, increase in population and also the high usage of portable electronic devices like mobile phones, laptops, the need for the progress of energy storage devices with high efficient, eco-friendly, long cycle stability has been attracted worldwide attention[1,2]. Supercapacitor (SC) is one of the important energy storage device due to their high power density, fast charging and discharging within seconds and long lifetime than batteries and greater energy density than conventional capacitors[3,4]. Supercapacitors finds applications in many energy storage fields such as hybrid electric vehicles, modern electronic devices, uninterruptible power supplies for computers, etc.,[5,6]. Based on the charge storage mechanism, SC can be classified into two types namely Electric double layer capacitor (EDLC) and Pseudocapacitor. In EDLC, the capacitance results from the non-faradaic charge storage mechanism between electrode and electrolyte interface and make use of carbon-based electrode materials such as porous carbon, reduced graphene oxide, aerogel, CNT, etc.,[7-10]. In pseudocapacitors, the capacitance results from the reversible faradaic charge storage mechanism occurring at the surface of the electroactive material[11,12]. Transition metal oxides like RuO_2, NiO, Fe_2O_3, MoO_3, $NiCo_2O_4$[(Ref.13-17)] and conducting polymers like polyaniline, polypyrrole, PEDOT:PSS [18-20] were used as electrodes in pseudocapacitors. Pseudocapacitors are more attracted due to their higher specific capacitance and energy density than EDLC [21,22].

Among the different metal oxides, manganese oxide has emerged as a promising electrode material due to its low cost, earth abundance, less toxicity, eco-friendly nature, multiple oxidation states and high theoretical capacitance (~1370 F/g) [23,24]. But due to its poor electronic conductivity (about 10^{-5} S cm^{-1}) and high charge transport resistance, it is difficult to utilize its high capacitance which also leads to the decay of capacitance during the charge/ discharge process[25,26]. Various researchers have implemented different approaches to improve the specific capacitance and cyclic stability of manganese oxide based supercapacitor. Manganese oxide can be prepared by various methods such as sol-gel method[27,28], co-precipitation method[29,30], hydrothermal method[31,32], thermal decomposition [33], Vapour-phase deposition [34,35], electrodeposition technique [36,37] and electrospinning technique [38].

Yang *et al.*[39], electrodeposited MnO_2 film on Ni foam through CV route attained a maximum specific capacitance of 2790 mF/cm^2 at a current density of

2 mA/cm^2 retained above 90% after 1000 cycles at 5 mA/cm^2. Similarly, Rusi *et al*., prepared α-MnO_2 through electrochemical deposition which showed a specific capacitance of 238 F/g at 1 mV/s scan rate with capacitance retention of 84% after 1900 times 40. But, Davoglio *et al*., reported a slightly high capacitance value of 289 F/g at 0.5 A/g and 88% cyclic stability after 10,000 cycles for α-MnO_2 particle synthesised at aqueous organic interface by microwave assisted method[41]. Xiaoyuzhao *et al*.[42], prepared δ-MnO_2 by hydrothermal method showed a specific capacitance of 571 F/g at current density of 0.2 A/g with capacitance retention of 91.4% after 1000 cycles. Likewise, Subramanian *et al*.[43], prepared MnO_2 by hydrothermal technique under mild conditions showed a specific capacitance of 168 F/g at 200 mA/g with cyclic efficiency of 83% for 100 cycles. Recently, Huang *et al*., synthesised nanoflower MnO_2 by facile chemical method and evaluated the electrochemical studies for different electrolytes. The specific capacitance of 171 F/g in KOH electrolyte at 1 A/g with 130.9% capacitance retention after 1000 cycles was reported[44].

In this work, manganese oxide (MO) was synthesised by chemical co-precipitation method and it was characterised for its functional group, phase structure, particle size and morphology by using FTIR, XRD, SEM and TEM. Additionally, its electrochemical properties like cyclic voltammetry (CV), galvanostatic charge/ discharge (GCD) and electrochemical impedance spectroscopy (EIS) were recorded. The specific capacitance of the prepared manganese oxide was found to be 116 F/g at current density of 1A/g. To augment its capacitance value, it was doped with a carbon material - multi-walled carbon nanotube (MWCNT) and a combination of conducting polymer poly (3,4-ethylenedioxy thiophene) polystyrene sulfonate (PEDOT:PSS) and MWCNT and their electrochemical performance were recorded. By doping MWCNT and PEDOT:PSS over MO, high specific capacitance of 537 F/g at a current density of 1A/g with 97% capacitance retention and coulombic efficiency of 98% over 10,000 cycles at a current density of 5 A/g.

Experimental Section

Materials

Manganese sulphate, sodium hydroxide, 1-methyl-2-pyrrolidone (NMP), and ethanol (99.9%) were purchased from Merck specialities Private Limited, India. Multi-walled carbon nanotube (MWCNT) was bought from Sisco Research Laboratory, India. Poly(3,4-ethylenedioxythiophene) polystyrene sulfonate (PEDOT:PSS), polyvinylidene difluoride (PVDF), acetylene black (AB) and nickel foam were obtained from Sigma Aldrich. All chemicals were of analytical grade and used as such without any further purification.

Synthesis of Manganese Oxide

A simple co-precipitation method was adopted for the preparation of manganese oxide (MO). 0.1 M manganese(II) sulphate and 0.2 M sodium hydroxide solutions were prepared for the preparation of MO. 100 mL of 0.2 M sodium hydroxide was added drop by drop to 100 mL of 0.1 M manganese sulphate with constant, continuous stirring at 80°C till the pH becomes 12 and the stirring was continued for about 2 h. After 2 h, brown precipitate obtained was filtered, washed with water and ethanol. It was dried for 8 h in hot air oven at 100°C and calcined at 500°C for 3 h to get manganese oxide (MO) [45,46].

Characterisation

The functional group of the prepared MO was analyzed by FTIR using Perkin-Elmer Spectrometer. The phase structure, crystallinity and particle size were determined by XRD (X'pert PRO analytical diffractometer) using Cu-K_α (λ= 1.514 Å) as radiation source. The morphological analysis of the prepared MO was investigated by SEM with EDAX using TESCAN (Bruker) microscope and TEM using FEI Tecnai 20 G2 microscope. The electrochemical performance of the active material was determined by electrochemical workstation Biologic SP-120.

Electrochemical characterisation

The active material, acetylene black and polyvinylidene difluoride was mixed and ground using mortar in the ratio 80:15:5. To this, a required amount of N-methyl-2-pyrrolidone was added to make a homogenous slurry. This slurry was coated on pre-treated nickel foam and then it was dried at 80°C for 12 h in an oven. After drying, it was uniformly pressed. The weight of the coated material (~3 mg) was maintained. The percentage composition and the mixing procedure for the active material of different electrode were given in Table 1.

All the electrochemical studies were performed with the three-electrode system. Active material coated on the nickel foam acts as working electrode,

Table 1 — Percentage Composition of different electrode materials

Electrode	% of Active material			Mixing procedure
	MO	MWCNT	PEDOT:PSS	
MO	80	-	-	MO was ground to powder
MO/MWCNT	75	5	-	MO was ball milled with MWCNT to obtain MO/MWCNT composite
MO/MWCNT/ PEDOT:PSS	75	2.5	2.5	MO was ball milled with MWCNT then PEDOT:PSS is added and ultrasonicated to get MO/ MWCNT/ PEDOT:PSS composite

Ag/AgCl(3 M KCl) and Pt wire acts as reference and counter electrode, respectively. The electrolyte used was 5 M potassium hydroxide. Cyclic voltammetry and galvanostatic charge-discharge studies were conducted with different scan rates from 5 mV/s to 50 mV/s with the potential range between 0 to 0.5 V and at different current densities from 1 to 5 A/g, respectively. Electrochemical impedance spectroscopy data was collected by applying an alternate current in the frequency range from 100 kHz to 10 mHz. The columbic efficiency can be calculated from GCD curve by using the following Eq. (1)

$$\eta = [\Delta t_D / \Delta t_C] \times 100\% \quad \ldots (1)$$

where, η is the columbic efficiency, t_D is the discharging time, t_c is charging time.

Results and Discussion

FTIR spectra

FTIR spectrum was recorded to confirm the functional group. Two peaks at about 621 and 516 cm^{-1} observed from Fig. 1. This may be due to the stretching vibration of Mn-O and Mn-O-Mn bonds[47,48] indicates the presence of MnO. The wide band at 3407 cm^{-1} is assigned to the OH stretching vibration. This may be due the absorption of water molecules in the atmosphere[49]. The absorption peak at 1109 cm^{-1} and 1633 cm^{-1} correspond to -OH bending vibrations may obtain as FTIR sample desk was prepared in an open air atmosphere[50,51].

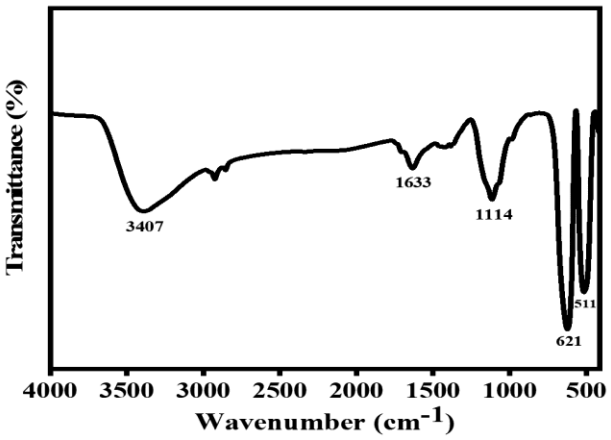

Fig. 1 — FTIR spectrum of manganese oxide

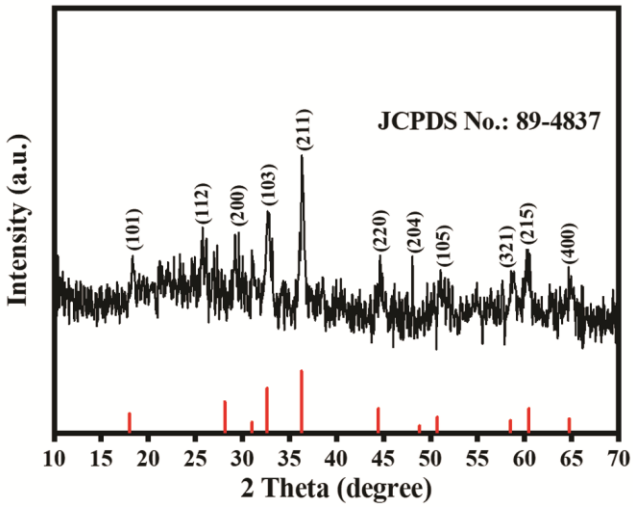

Fig. 2 —XRD (black) and its corresponding JCPDS plots (red) of manganese oxide

XRD analysis

X-ray diffraction pattern of the prepared MO is shown in Fig. 2. The diffraction peaks observed at 2θ values of 18.2°, 25.7°, 29.5°, 32.7°, 36.3°, 44.6°, 51.4°, 58.8°, 60.4° can be assigned to (101), (112), (200), (103), (211), (220), (105), (321)and (224) planes, respectively. All these diffraction peaks are indexed to the standard pattern of body centered tetragonal Mn_3O_4 (JCPDS No. 89-4837) having lattice constant with the space group I41/amd. No other peak can be seen indicates the purity of the prepared MO. The sharp peak indicates the crystallinity nature of the MO. By using Debye-Scherrer equation (2), the average crystallite size was calculated from the high intensity peak[52]

$$D = K\lambda / \beta cos\theta \quad \ldots (2)$$

where D (nm) is the crystallite size, K is diffraction constant (~0.9), λ is wavelength of the incident X-ray, β is the full-width half-maximum multiplies and θ is the angle of diffraction. The average crystallite size was found to be 5.9 nm.

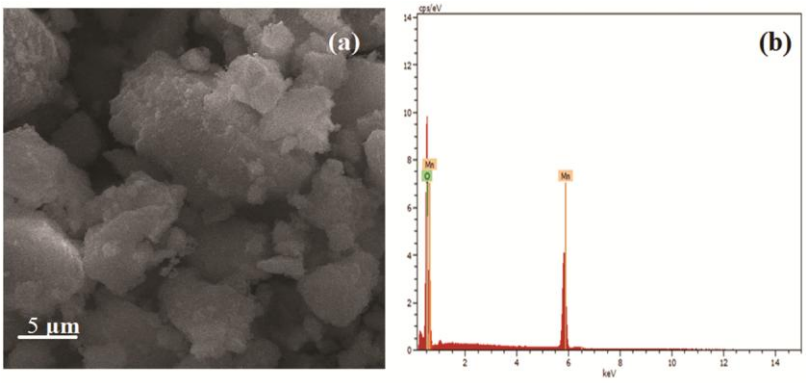

Fig. 3 — (a) SEM Image and (b) EDAX spectrum of manganese oxide

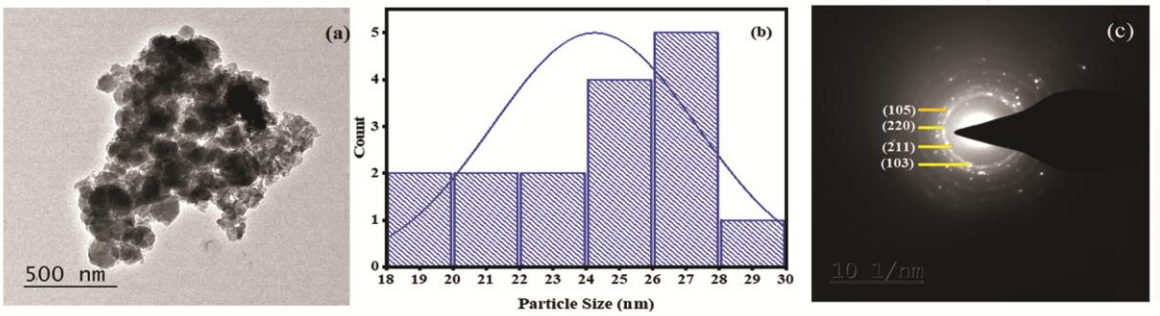

Fig. 4 — (a) TEM image (b) histogram and (c) SAED of manganese oxide

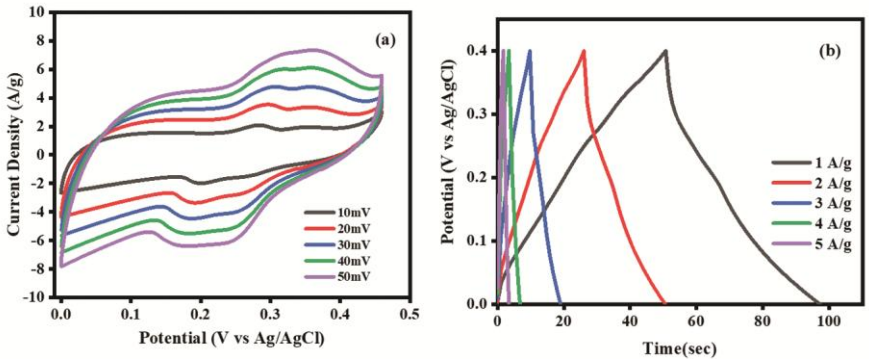

Fig. 5 — (a) CV and (b) GCD curve of manganese oxide at various scan rates and current densities

Morphological Analysis

The surface morphology of the prepared MO was examined by SEM with EDAX analysis and is shown in Fig. 3. Spherical like crystals is observed in Fig. 3a. The presence of predominant characteristic elemental peak namely manganese and oxygen in Fig. 3b confirms the presence of MO is in pure form.

The magnified surface morphology of the prepared MO was further confirmed by TEM image. The images of TEM and SAED are shown in Fig. 4. The SAED pattern of the MO shows the concentric circles which confirm the polycrystalline nature and (103), (211), (220) and (105) planes are consistent with results obtained by XRD.

Electrochemical Characterisations

Electrochemical performance on doping MWCNT, PEDOT:PSS with MO

The CV and GCD curves of MO at different scan rates and current densities are shown in Fig. 5. The increase in the area under CV curve with increase in scan rate may be due to the diffusion rate of electrolyte ions. The redox peak with the potential window of 0 to 0.5V indicates the pseudo-capacitance

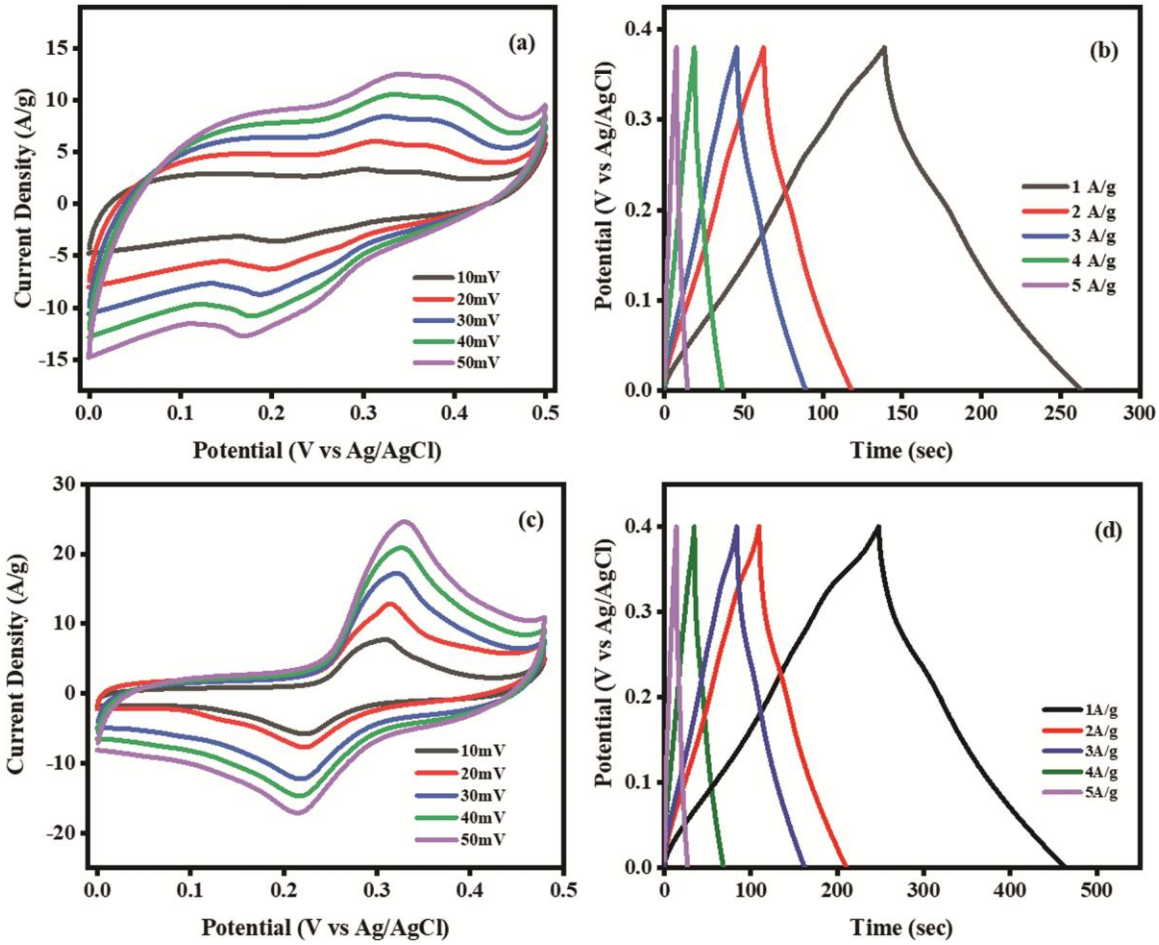

Fig. 6 — CV and GCD curves of (a, b) MO/MWCNT and (c, d) MO/MWCNT /PEDOT:PSS at different scan rates and current densities

behaviour of MO. The GCD of MO at different current densities are displayed in Fig. 5b. From the discharge curve of GCD, the specific capacitance of MO at different densities can be calculated using Eq. (3)[Ref. 53]

$$C = I\Delta t/m\Delta V \quad \ldots (3)$$

where 'C' is the specific capacitance of the electrode material (F/g), 'I' is the applied current for charge-discharge cycles (A), 'Δt' is the discharge time (sec), 'm' is the mass of the working electrode (g) and 'ΔV' is the operating potential window (V). The specific capacitance of MO was 116, 107, 70, 33, 21 F/g at current densities of 1, 2, 3, 4, 5 A/g. A low capacitance value at high current density is observed. This may be due to the reduced diffusion time of the electrolyte ions at high current density- only the outer surface of the active material can be easily accessed and it is difficult to access the interior surface of the active material. At low current density, the diffusion time of the electrolyte ions is sufficient to access the inner and outer surface of the active material which leads to the high capacitance value.

The individual CV and GCD curves of MO/MWCNT and MO/MWCNT /PEDOT:PSS at different scan rates and current densities are shown in Fig. 6. The calculated specific capacitance values of the electrode material were given in Table 2. An increase in specific capacitance value from MO to MO/MWCNT/PEDOT:PSS is clearly observed. A minimum amount of the dopant added to MO increases the electroactivity of the electrode material. The specific capacitance of the MO/MWCNT/ PEDOT:PSS shows the highest value when compared to all other electrodes. It can be noted that the doping of minimum amount of MWCNT along with PEDOT:PSS to MO shows the highest specific capacitance value.

The CV and GCD curve of bare nickel foam, MO, MO/MWCNT, MO/MWCNT/PEDOT:PSS electrode materials at scan rate of 10 mV/s and at a

current density of 1 A/g are depicted in Fig. 7. The CV curve exhibits the redox behaviour proving the presence of faradaic charge storage mechanism. The influence of addition of MWCNT, PEDOT:PSS to MO and the electrochemical behaviour can be detected from the Fig. 7. The electrochemical activity of the nickel foam shows negligible.

Furthermore, the galvanostatic charge/discharge curve also confirms the faradaic nature of the active material. The higher discharge time of MO/ MWCNT/PEDOT:PSS leads to higher specific capacitance compared to MO at current density of 1 A/g. The calculated specific capacitance of MO/ MWCNT/PEDOT:PSS at current density of 1 A/g is 537 F/g, which is higher than MO of 116 F/g at 1 A/g. The porous nature, high surface area, good chemical stability of MWCNT and high electrically conductive of PEDOT:PSS polymer along with the metal oxide attains the higher specific capacitance value[54,55]. The specific capacitance of all the active material as a function of different current densities is displayed in Fig. 8a. This clearly shows the enhancement inthe specific capacitance of MO due to the doping effect.

Table 2 — Specific capacitance value with current density of the electrode materials

Current density(A/g)	Specific capacitance (F/g)		
	MO	MO/MWCNT	MO/MWCNT/ PEDOT:PSS
1	116	312	537
2	107	272	503
3	70	244	464
4	33	178	378
5	21	98	265

EIS analysis

The Impedance spectra was recorded for the three electrodes (MO, MO/MWCNT, MO/MWCNT/ PEDOT:PSS) and presented as Nyquist plot in the Fig. 8b. At low frequency region, a straight line is observed for all the electrodes which implies the charge transfer resistance is low[49]. This indicates the ideal pseudocapacitive behaviour of the electrode material. The solution resistance (R_s) of the MO, MO/MWCNT and MO/MWCNT/ PEDOT:PSS electrode material obtained from the Nyquist plot is 0.548 Ω, 0.48 Ω and 0.397 Ω, respectively. It can be observed that MO/MWCNT/ PEDOT:PSS electrode has low R_s value compared to other electrode materials. These results are in good agreement with CV and GCD analysis, which proves that MO/MWCNT/PEDOT:PSS electrode has low resistance, high specific capacitance value that makes easy access for the charge and discharge process between electrode and electrolye.

Electrochemical Stability

The electrochemical stability of the electrode materials was analysed by performing GCD for 10,000 cycles at a current density of 5 A/g. Fig. 8 (c) shows the cyclic stability of MO/MWCNT/ PEDOT:PSS for 10,000 cycles at 5A/g. It can be noticed that 97% of initial capacitance retention was retained with high coulombic efficiency of 98% over 10,000 cycles. A high stability was achieved by MO/MWCNT/ PEDOT:PSS electrode material. To compare our results with reported values, a comparative table is provided in Table 3 with specific capacitance and cycle life of MO based electrode materials.

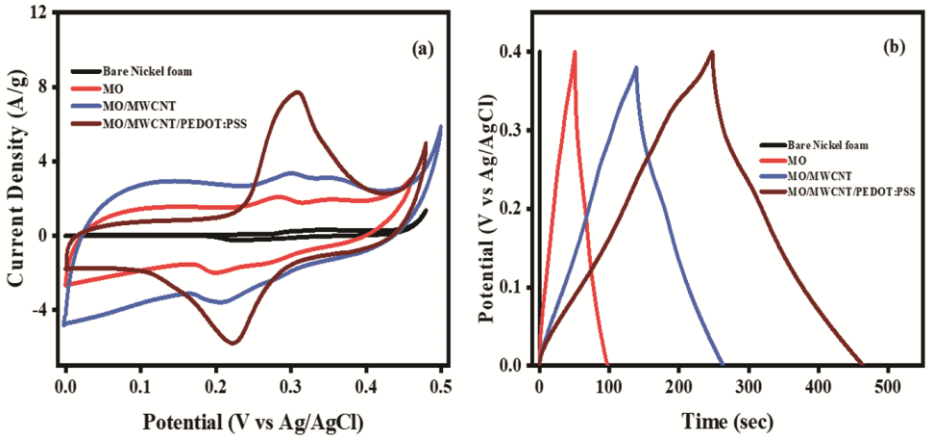

Fig. 7 — (a) CV and (b) GCD curve of bare Nickel foam, MO, MO/MWCNT, MO/MWCNT/ PEDOT:PSS at scan rate of 10 mV/s and current density of 1 A/g

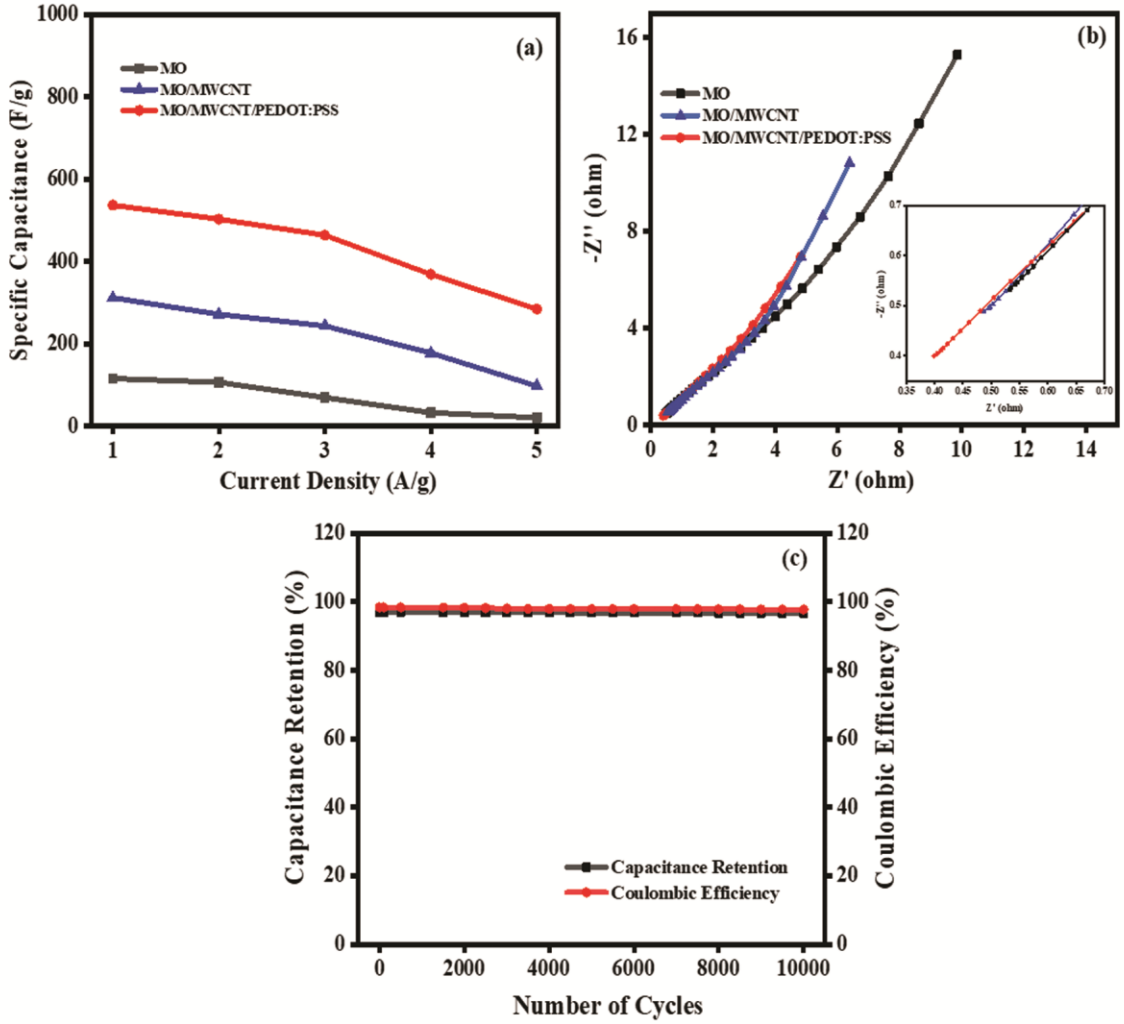

Fig. 8 — (a) Specific capacitance as a function of current density, (b) Nyquist Plot (insets are the magnified view at high frequency region) and (c) cyclic Stability of MO/MWCNT/PEDOT:PSS for 10,000 cycles at 5 A/g

Table 3 — Comparative table of specific capacitance and cycling stability of MO based electrode materials

S. No.	Electrode material	Electrolyte	Specific capacitance	Cycling stability	Ref.
1.	α-MnO_2	1 M Na_2SO_4	289 F/g at 0.5A/g	88% over 10,000 cycles	[41]
2.	Mn_3O_4	1 M Na_2SO_4	322 F/g at 0.5mA/cm^2	77% over 1000 cycles	[56]
3.	Mn_3O_4/AC	2 M $TEABF_4$	216 F/g at 0.5A/g	85% 0ver 500cycles	[57]
4.	MnO_2/CNT	1 M Na_2SO_4	115 at 0.5 A/g	95% over 1000 cycles	[58]
5.	MnO_2/CNT	1 M Na_2SO_4	201 F/g at 1 A/g	10,000 cycles	[59]
6.	MnO_2/MWCNT	0.5 M Na_2SO_4	162.2 F/g at 0.2A/g	90% over 2000 cycles	[60]
7.	MnO_2/MWCNT	1 M Na_2SO_4	171 F/g at 1A/g	90% over 2000 cycles	[61]
8.	α-Mn_2O_3/ PEDOT:PSS	1 M LiPF6 in mixture of ethylene carbonate and ethyl carbonate	1450 mAh/g at 100 mA/g	200 cycles	[62]
9.	PEDOT:PSS/MnO_2/CNT	1 M Na_2SO_4	261 F/g	----	[63]
10.	Mn_3O_4/ MWCNT/ PEDOT:PSS	5 M KOH	537 F/g at 1A/g	97% over 10,000 cycles	This work

Conclusion

Manganese oxide (MO) was synthesized by a simple chemical co-precipitation method. XRD pattern confirms the formation of tetragonal structure with the crystallite size of 5.9 nm. SEM and TEM analysis shows the crystalline nature of MO and the elemental composition confirms the presence of Mn and O. The electrochemical performance of the MO

showed a specific capacitance of 116 F/g at a current density of 1A/g. To augment its electrochemical performance, it was doped with MWCNT and PEDOT:PSS. The specific capacitance value of MO/MWCNT is 312 F/g at a current density of 1 A/g. MO/MWCNT/PEDOT:PSS electrode shows a very high specific capacitance value of 537 F/g at a current density of 1A/g with good rate performance retained with an excellent electrochemical stability of 97% capacitance retention and coulombic efficiency of 98% over 10,000 cycles at a current density of 5 A/g. This study shows the excellent performance of MO/MWCNT/PEDOT:PSS electrode suitable for supercapacitor applications.

References

1 Wenhua Z, Ruizhi L, Cheng Z, Yuanyuan L, Jianlong X & Jinping L, *Adv Sci*, 4 (2017) 1600539.
2 Rudra K, Prabhakar R & Ashutosh S, *J Mater Chem A*, 4 (2016) 9822.
3 Conway B E, Electrochemical Supercapacitors: Scientific Fundamentals and Technological Applications, Kluwer Acedamic/Plenum Publishers, New York, (1999).
4 Miller J R & Simon P, *Science*, 321 (2008) 651.
5 Young S Y, Se Y C, Jinyong S, Byung H K, Sung-Jin C, Seung J B, Yun S H, Yongsug T, Yung W P, Sungjin P & Hyoung-Joon J, *Adv Mater*, 25 (2013) 11.
6 Yong Z, Hui F, Xingbing W, Lizhen W, Aiqin Z, Tongchi X, Huichao D, Xiaofeng L & Linsen Z, *Int J Hydrog Energy*, 34 (2009) 4889.
7 Songhun Y, Jinwoo L, Taeghwan H & Seung M, *J Electrochem Soc*, 147 (2000) 2507.
8 Jagdees P, Ashwani K S, Jyoti S, Kotnala R K & Kedar S, *Mater Res Express*, 5 (2018) 055028.
9 Wencui L, Reichenauer G & Fricke J, *Carbon*, 40 (2002) 2955.
10 Wei C, Zhongli F, Lin G, Xinhe B & Chunlei W, *Chem Commun*, 46 (2010) 3905.
11 Weifeng W, Xinwei C, Weixing & Ivey D G, *Chem Soc Rev*, 40 (2011) 1697.
12 Simon P & Gogotsi Y, *Nat Mater*, 7 (2008) 845.
13 Hui X, Ying S M, Guoliang Y, Chong C & Li L, *Electrochem Solid-State Lett*, 15 (2012) A60.
14 Sun I K, Jung-Soo L, Hyo-Jin A, Hyun-Kon S & Ji H, *ACS Appl Mater Interfaces*, 5 (2013) 1596.
15 Kulal P M, Dubal D P, Lokhande C D & Fulari V J, *J Alloys Compd*, 509 (2011) 2567.
16 Wei T, Lili L, Shu T, Lei L, Yunbo Y, Yuping W & Kai Z, *Chem Commun*, 47 (2011) 10058.
17 Santosh J U, Chaudhari G N, Bodade A B & Mardikar S P, *Mater Sci Energy Technol*, 3 (2020) 289.
18 Na L, Yinghong X, Chongzheng X, Huihui L & Xiaodi Y, *Int J Electrochem Sci*, 8 (2013) 1181.
19 Yang H, Hongfei L, Zifeng W, Minshen Z, Zengxia P, Qi X, Yan H & Chunyi Z, *Nano Energy*, 22 (2016) 422.
20 Xing G, Lei Z, Xiaomin C, Ce L, Huiqin L, Yang L, Xiaodong W & Xiuguo C, *Nanomaterials*, 8 (2018) 335.
21 Mathieu T & Thierry B D B, *Chem Mater*, 16 *(*2004) 3184.
22 Yong Z, Hui F, Xingbing W, Lizhen W, Aiqin Z, Tongchi X, Huichao D, Xiaofeng L & Linsen Z, *Int J Hydrog Energy*, 34 (2009) 4889.
23 Ming H, Fei L, Fan Dong, Yu Xin Z & Li Z, *J Mater Chem A*, 3 (2015) 21380.
24 Banafsheh B & Ivey D G, *J Power Sources*, 196 (2011) 10762.
25 Yongchuan L, Dawei H, Jiahua D, Yongsheng W & Shulei L, *Mater Chem Phys*, 147 (2014) 141.
26 Dawoud H D, Tahtamouni T A & Bensalah N, *Int J Energy Res*, 43 (2019) 1.
27 Reddy R N & Reddy R G, *J Power Sources*, 124 (2003) 330.
28 Xingyan W, Xianyou W, Weiguo H, Sebastian P J & Gamboa S, *J Power Sources*, 140 (2005) 211.
29 Mathieu T, Thierry B & Belanger D, *Chem Mater*, 14 (2002) 3946.
30 Prasada R T, Kumar A, Naik V M & Naik R, *J Alloys Compd*, 789 (2019) 518.
31 Subramanian V, Zhu H, Robert V, Ajayan P M & Wei B, *J Phys Chem B*, 109 (2005) 20207.
32 Tang X, Li H, Liu Z H, Yang Z & Wang Z, *J Power Sources*, 196 (2011) 855.
33 Shuijin L, Kaibin T, Zhen F, Qiangchun L & Huagui Z, *Mater Lett*, 60 (2006) 53.
34 Chang Y Q, Yu D P, Long Y, Xu J, Luo X H & Ye R C, *J Cryst Growth*, 279 (2005) 88.
35 Banis M N, Zhang Y, Banis H N, Li R, Sun X, Jiang X & Nikanpour D, *Chem Phys Lett*, 501 (2011) 470.
36 Fan X , Wang X, Li G, Yu A & Chen Z, *J Power Sources*, 326 (2016) 357.
37 Mishra P K,Prajapati C S, Shahi R R, Kushwaha A K & Sahay P P, *Ceram Int*, 44 (2018) 5710.
38 Sahoo B & Panda P K, *J Adv Ceram*, 2 (2013) 26.
39 Yang J, Lian L, Ruan H, Xie F & Wei M, *Electrochim Acta*, 136 (2014) 189.
40 Majid S R, *Solid State Ion*, 262 (2014) 220.
41 Davoglio R A,Cabello G, Marco J F & Biaggio S R, *Electrochim Acta*, 261 (2018) 428.
42 Zhao X, Hou Y, Wang Y, Yang L, Zhu L, Cao R & Sha Z, *RSC Adv*, 7 (2017) 40286.
43 Subramanian V, Zhu H & Wei B, *J Power Sources*, 159 (2006) 361.
44 Huang Y, Weng D, Kang S & Lu J, *J Nanosci Nanotechnol*, 20 (2020) 4815.
45 Gowda J I, Hanabaratti R M & Hipparagi S S, *Results Chem*, 5 (2023) 100801.
46 Gowda J I, Hanabaratti R M, Pol P D, Sheth R C, Joshi P P & Nandibewoor S T, *Chem Data Collect*, 38 (2022) 100824.
47 Chen H & He J, *J Phys Chem C*, 112 (2008) 17540.
48 Mylarappa M, Lakshmi V V, Mahesh K V, Nagaswarupa H P & Raghavendra N, *IOP Conf Ser: Mater Sci Eng*, 149 (2016) 012178.
49 Kumar Y, Chopra S, Gupta A, Kumar Y, Uke S J & Mardikar S P, *Mater Sci Energy Technol*, 3 (2020) 566.
50 Zheng M, Zhang H, Gong X, Xu R, Xiao Y, Dong H, Liu H & Liu Y, *Nanoscale Res Lett*, 8 (2013) 166.
51 Manigandan R, Suresh R, Giribabu K, Vijayalakshmi L, Stephen A & Narayanan V, *AIP Conf Proc*, 1576 (2014) 125.
52 Murty B S, Shankar P, Raj B , Rath B B & Murday J, *Textbook of Nanoscience and Nanotechnology*, First edition, (Universities Press Private Limited, India), 2013.

53 Singu B S, Goda E S & Yoon K R, *J Ind Eng Chem*, 97 (2021) 239.
54 Chen W, Fan Z, Gu L, Bao X & Wang C, *Chem Commun*, 46 (2010) 3905.
55 Sonia T S, Mini P A,Nandhini R, Sujith K, Avinash B, Nair S V & Subramanian K R V, *Bull Mater Sci*, 36 (2013) 547.
56 Gnana S R B, Asiri A M, Wu J J & Anandan S, *J Alloys Compds*, 636 (2015) 234.
57 Bui P T M, Song J H, Li Z Y, Shaheer A M & Yang O B, *J Alloys Compds*, 694 (2017) 560.
58 Tan D Z W, Cheng H, Nguyen S T & Duong H M, *Adv Funct Mater*, 29 (2014) A107.
59 Li L, Zhong A H, Ning A, Yu Y Y, Zhi M L & Hong Y W, *J Phys Chem C*, 118 (2014) 22865.
60 Wang H, Peng C, Peng F, Yu H & Yang J, *Mater Sci Eng B*, 176 (2011) 1073.
61 Huang Y, Weng D, Kang S & Lu J, *J Nanosci Nanotechnol*, 20 (2020) 4815.
62 Ko I H, Kim S J, Lim J, Yu S H, Ahn J, Lee J K & Sung Y E, *Electrochim Acta*, 187 (2016) 340.
63 Liu L & Choi S, *ACS Appl Energy Mater*, 3 (2020) 10224.